Chapter 6

Wideband Imaging Polarimetry of Field Stars Behind Bok Globules

6.1 Introduction

Among the wide range of molecular clouds found in the Galaxy, Bok globules (Bok & Reilly 1947) occupy the lowest rung, because of their small physical sizes (typically, less than a parsec) and masses (a few to several tens of solar masses). Time and again, the dynamical and structural simplicity of these clouds and their isolation from contaminating environments, have been upheld in support of their suitability as laboratories for studying the behavior of a spherical cloud under the action of self-gravitation (Kenyon & Starrfield 1979; Dickman & Clemens 1983). Though several decades have passed since the first catalogue of such clouds was compiled (Barnard 1991), pretty little is still understood about the processes leading to their formation and subsequent evolution.

Schneider & Elmegreen (1979) observed the tendency of low density filamentary clouds in the interstellar medium to condense into clumps and globules under gravity and magnetic field (see also Leung et al 1982). Another scenario for the formation of Bok globules was put forward by Reipurth (1982), in which ionizing radiation from a new-born star sweeping across a clump in the surrounding molecular cloud, causes the clump to implode and eventually evolve into a globule (Patel et al 1993). However, the presence of magnetic fields are necessary to prevent the clump from being completely evaporated off by the ionizing front before it can settle into an equilibrium configuration (Bertoldi & McKee 1990). Magnetic fields are also supposed to considerably influence the dynamics of the globules and the formation of structures in them (Mouschovias 1976; Myers & Goodman 1988b, 1988b; Ryden 1996).

About half a century ago, Bart Bok had speculated that these globules could be seats of low-mass star formation. The prediction has now been vindicated with observational evidences showing that a large fraction of the Bok globules should be forming stars (Yun & Clemens 1990, 1994a). Bok globules offer a unique testbed to

confront theory with observations – a small, closely spherical gas cloud collapsing under gravity to form a single star. Magnetic fields are known to play key roles during the star-forming processes by mediating accretion, directing the outflows and collimating the jets.

The imprints which the processes of globule and star formation leave on the ambient Galactic magnetic field provide a valuable handle for understanding these phenomena. But, observing the three dimensional spatial structure of the magnetic field in an interstellar cloud is a tricky business (Myers & Goodman 1991, MG hereafter), so is deducing the strength of the field (Goodman et al 1989). Optical polarimetry of starlight scattered by magnetically aligned dichroic dust grains at the periphery of these globules, has been widely employed to determine the two dimensional structure of magnetic fields (as projected in the plane of the sky) associated with the globules. The underlying mechanism which polarizes starlight was proposed by Davis and Greestein (1951) and later improved upon by several others (Purcell 1979, Mathis 1986). As a result of this mechanism, initially unpolarized starlight, passing through a cloud of dichroic dust grains will become partially polarized with the electric field vector parallel to the direction of the magnetic field.

Single aperture photometric techniques which were earlier adapted for doing polarimetry (Serkowski 1975), were incapable of achieving the sensitivity and angular resolution, which is required to quantitatively understand the magnetic field patterns. This situation has now completely changed, with the widespread introduction of two dimensional detectors into astronomy. The great advantages of the imaging mode of observations over the single aperture techniques (large spatial multiplexing capability, high angular resolution, manifold improvement of sensitivity, simultaneous sky measurement etc.) have made polarimetry at optical and infrared wavelengths, a mainstream astronomical technique (Scarrott 1991; Kane et al 1995).

Here, we present the results of imaging polarimetric observations of three Bok globules. These globules were selected from a catalogue of 248 small ($\phi < 10'$) molecular clouds identified from Palomar Observatory Sky Survey (POSS) prints, by Clemens and Barvainis (1988, CB hereafter).

6.2 Observations

The data for this study was collected during three observation runs – first one in November 1996 (CB 16 and CB 17), second in February 1997 (CB 60) and third in December 1997 (CB 3, CB 25 and CB 54). The observations were made with IMPOL mounted on the 1.2 m GIRT telescope on Mt. Abu. The relevant details of the observation technique and the analysis of raw data to extract polarimetric information, are discussed in the following subsections.

6.2.1 The Data

For each cloud, sixteen five minute exposures were taken, in four sets; each set consisting of four exposures taken at four different orientations of the half-wave plate (HWP), namely 0°, 22.5°, 45°, and 67.5°. Starting from 0°, the orientation of the HWP was incremented by 22.5°, after every exposure till one at 67.5° is taken. Then the cycle is again started from 0°. While taking each exposure, the telescope pointing was dithered with a frequency of about 0.5 Hz, so that the point-spread function has an FWHM of about 3 pixels. The need for doing the cycling process and dithering is discussed below. CB 3, CB 25, CB 16, CB 17 and CB 54 could be covered in one field of the instrument, while CB 60 had to be covered with two fields.

Polarimetry is almost always photon-starved – the more the number of photoelectrons collected, the better the accuracy is – until, of course, the instrumental polarization floor is reached. In order to increase the signal collected for a given exposure time, we have used a wideband filter (made of Schott KG3 glass), which has a passband approximately equivalent to the combined V and R bands. This does not affect the observations, because we are mainly interested in the average properties of the magnetic field pattern and not on the wavelength dependence of polarization. Besides, it is known that the polarization due to dichroic scattering do not change appreciably over optical wavelengths.

For each object within the field of view, two images, called the ordinary and the extraordinary, separated by about 33 pixels, is formed on the CCD. These two images correspond to two orthogonal linear polarization components that are measured simultaneously. The ratio (R) of the difference between the fluxes collected in the two images to their sum, at different orientations (α) of the HWP, are related to the normalized Stokes parameters as

$$R(0°) = -R(45°) = q \qquad \text{and} \qquad R(22.5°) = -R(67.5°) = u \ . \tag{6.1}$$

The degree of linear polarization (p) and its position angle (θ) measured with respect to a fiducial direction, are related to the normalized Stokes parameters through the relation

$$R(\alpha) = p \cos\left(2\theta - 4\alpha\right) \ . \tag{6.2}$$

Photometry of stellar images in each of the sixteen frames is carried out using the tasks available in the DIGIPHOTX package in IRAF[1]. Stellar image pairs, corresponding to orthogonal polarization components of the light from each star, are identified in each frame and the ratio R calculated for each of the image pairs in all the sixteen frames. In order to estimate p and θ, all the sixteen values of R, thus obtained, are fit simultaneously to a cosine curve of the form in Eqn. 6.2, using a χ^2-fitting technique. An estimate of the error in determining the ratios (R's), which is required to calculate

[1]IRAF is distributed by National Optical Astronomy Observatories, which are operated by the Association of Universities for Research in Astronomy, Inc, under contract with the National Science Foundation.

the χ^2 statistic during fitting, is obtained from the standard deviation of the multiple measurements which are available at each position of the HWP.

There are two effects which are to be taken care of while determining the ratios. Firstly, the two channels of the polarimeter will have different sensitivities, by virtue of their orthogonal polarization states. Besides, the sensitivity varies from pixel to pixel of the CCD. The two effects become coupled if the images move on the CCD surface while the exposures are taken and worse still, if the point-spread function is undersampled. The effects due to pixel to pixel sensitivity variations can be eliminated by ensuring that the images do not move on the CCD surface during the time in which a set of exposures at the four orientations of the HWP is taken. Once the effects of image motion has been taken care of, the channel to channel sensitivity variation (hereafter denoted by F), can be estimated by a suitable combination of the eight flux values obtained from a set of exposures at the four orientations of the HWP (see Sec. 3.1.3). This exploits the fact that these flux values are not actually independent, but are related to each other as indicated in Eq. 6.1 above. Before calculating the ratios ($R's$), the individual flux values in each stellar image pair are corrected for the channel to channel sensitivity difference.

The instrument's off-axis auto-guidance system is capable of giving subarcsecond tracking accuracy with guide stars as faint as V = 15. Besides, it also allows to dither the telescope pointing, while an exposure is being taken, so as to ensure that the FWHM of the point-spread function is sufficiently large to give proper sampling. It was found that an FWHM $\gtrsim 3$ pixels is sufficient to keep the effects of any residual image motion, at adequately low levels (see Sec. 5.1.1). And finally, the cycling of exposures between the four HWP orientations, mentioned in the previous section, is meant to ensure that the four exposures are spaced apart in as little time as is possible. Some polarimeters do follow the strategy of observing all the four polarization components in one exposure, but by paying the cost for it, being able to cover only less than a quarter of the field at a time (see for example, Geyer and Jockers 1993). The two channel technique employed in this instrument is a compromise between the two competing requirements.

The parameter F, discussed above, is also very useful as a diagnostic aid in the identification of stellar images which are contaminated by the presence of other nearby bright sources, edge effects on the CCD etc. We find that, whenever the value of F estimated for a star lies below 0.9 or above 1.1, it is useful to check the data directly for the presence of such effects.

Measurements in the laboratory as well as with standard stars indicate that the self-polarization of the instrument is at the level of about 0.03% and that polarimetric accuracy is limited by photon-noise for observations of stars as faint as $17^{\rm th}$ to $18^{\rm th}$ magnitude in the V-band. An estimate of the error in the measurement of p based on photon noise alone is given in Eqn. 3.14, which is repeated below.

$$\sigma_p = \frac{\sqrt{N + N_{\rm b}}}{N} \qquad \text{and} \qquad \sigma_\theta = 0.5 \times \frac{\sigma_p}{p} \text{ rad} \tag{6.3}$$

where N and $N_{\rm b}$ are the fluxes from the star and the background respectively. The

data corresponding to a star, for which the polarimetric error obtained by the fitting technique is much more than that estimated from photon noise as above, is considered suspect and closer inspection of the data is made, with the intention of eliminating stars with spurious effects.

The photometric aperture used for determining the fluxes in the stellar images, typically, has a radius close to the FWHM of the point-spread function. Actually, polarimetry is carried out using a few photometric software apertures with radii close to the FWHM. From among the values of polarization thus obtained, the one which is associated with the minimum error is accepted as the best estimate. As shown in Eqn. 6.3, the error, due to photon noise, in estimating θ is inversely proportional to the signal to noise ratio in the measurement of p. Polarization measurements of all stars with $\sigma_\theta \gtrsim 15$ are treated as insignificant and eliminated from further calculations. It is well-known that the value of p obtained from Stokes parameter measurements, is a biased estimator and several debiasing schemes have been suggested in the literature (see for example Clarke et. al. 1983, Simmons & Stewart 1984). Nevertheless, for $\frac{p}{\sigma_p} \gtrsim 4$, all the dibiasing schemes are well-approximated by the single equation

$$\hat{p}_0 = p\sqrt{1 - \frac{\sigma_p^2}{p^2}}\ , \tag{6.4}$$

where $\hat{p}_0$ is the "debiased" estimate of the true degree of linear polarization p_0.

6.3 Results

All the globules, which are studied here, are seen in the Palomar Observatory Sky Survey (POSS) prints and are listed in the catalog of small molecular clouds (optical sizes smaller than about 10 arcminutes) published by Clemens and Barvainis (1988 CB hereafter). A literature survey based on the SIMBAD database did not show any previous published record of optical polarimetry of these clouds. All globules are close to the Galactic disk, with Galactic latitudes less than about 4°; the optical sizes as quoted by CB are given in Table 6.6. The core of CB 16 appears thin and elongated, with its long axis oriented about 110° east of north. There is an irregularly shaped shell of brighter material around the core which is apparently connected on the western side to a long serpentine filament, that continues southward of the cloud. CB 17 appears about $12'$ towards northeast of CB 16. Both CB 17 and CB 25 are similar in appearance – a very dense core surrounded by a brighter shell. In CB 17 the shell has a small extension at about 30° east of north. CB 54 and CB 60 appear as fairly circular regions with relatively fewer number of stars than their surroundings and having a patchy appearance on the Palomar prints.

The upper parts of figures 6.1-6.3 show maps of polarization vectors superimposed on Digitized Sky Survey images of the cloud regions. The lines at the north-east corner of the maps give the general direction of the Galactic plane in the region. The bottom parts of figures 6.1-6.3 show plots of the error in polarization measurement for each

star against its V-band magnitude, for the three clouds. For all clouds except CB 17 and CB 25, we find that the polarimetric uncertainties are less than 0.5% for stars as faint as V=16.2 magnitude. The data of CB 17 and CB 25 are slightly worse, but the uncertainties in p are still smaller than 1% for stars at V=16.5 magnitude. However, for all the stars listed, the polarization measurement is significant at least at 2σ level. Figures 6.4(a) and (b) and Fig. 6.5 show the polarization maps for CB 3, CB 25 and CB 54. In these figures, the direction of the local Galactic magnetic fields are indicated by the encircled vectors, which show the scale of the vectors as well.

Tables 6.1-6.4 present the data corresponding to the polarization maps. Column (1) of the table contains a sequence number for identifying the stars. In table 6.2, many stars have a second number following the identification sequence number. This corresponds to the quadrant in which the star falls, as described in Sec. 6.4.1. Columns (2), (3), (4) and (5) list the measured degree of linear polarization (p), the polarization position angle (θ) and the 1σ uncertainties in determining these quantities through the fitting procedure. The V-band magnitudes presented in column (6) are obtained by calibrating the aperture magnitudes with the values available for those stars present in the HST Guide Star Catalogue.

In order to ascertain that the polarization measured is mainly due to the scattering of starlight by the dust grains in the cloud and not in the intervening interstellar medium, we need to know the distance to the clouds. In the absence of published estimates of distances to these clouds, an alternative is to use the average value of 600 pc obtained by CB for their sample of clouds. Another method, which is due to Herbst and Sawyer (1981), employs the number (n) of foreground stars appearing over an area corresponding to a$'$ over the cloud in Palomar blue prints, to estimate the distance (d) to the cloud using the relation

$$d = 320(n\frac{a_5}{a})^{0.57} \text{ pc} , \tag{6.5}$$

where a_5 is the area of a circle with $5'$ diameter. On employing this technique, we get a distance of about 400 pc to the clouds..

Serkowski et. al. (1974) have observed the following relation between the maximum degree of linear polarization introduced into light from stars by the interstellar dust grains and the visual extinction suffered by the light.

$$p_{\max}(\%) \leq 2.7A_{\rm V} \text{ (mag)}. \tag{6.6}$$

Using a value of $A_{\rm V} = 1$ mag. per kpc for the extinction in the interstellar medium, this relation translates to

$$p_{\max}(\%) \leq 2.7d \text{ (kpc)} , \tag{6.7}$$

where d is the distance traveled by light in the interstellar medium. Even if we accept the more conservative estimate of 600 pc as the distance to these clouds, the upper limit on interstellar polarization is only about 1.6%. Since the observed polarization values are more (see Fig. 6.6 and 6.7) than the upper limit predicted for scattering in the interstellar medium at these distances, the highly uniform fields of CB 16, CB 17

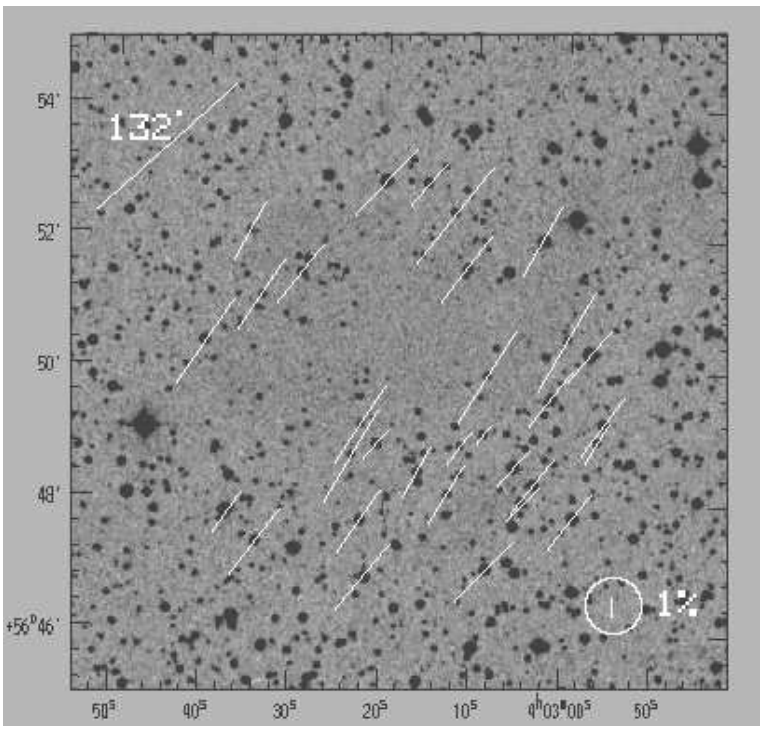

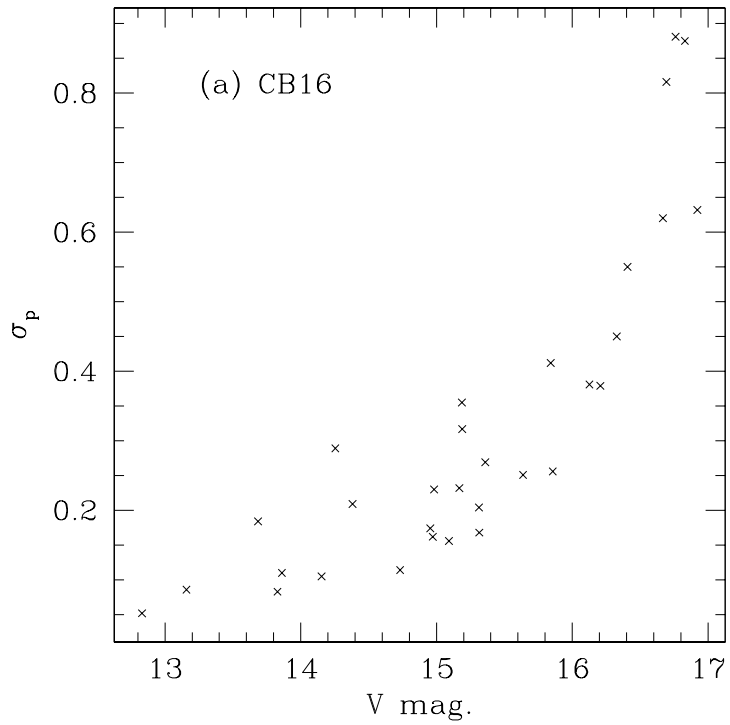

Figure 6.1: (Top) Polarization vector map of the field stars shining through the dust near the dark globule CB 16. (Bottom) Error in polarization measurement of each star plotted against its V-band magnitude.

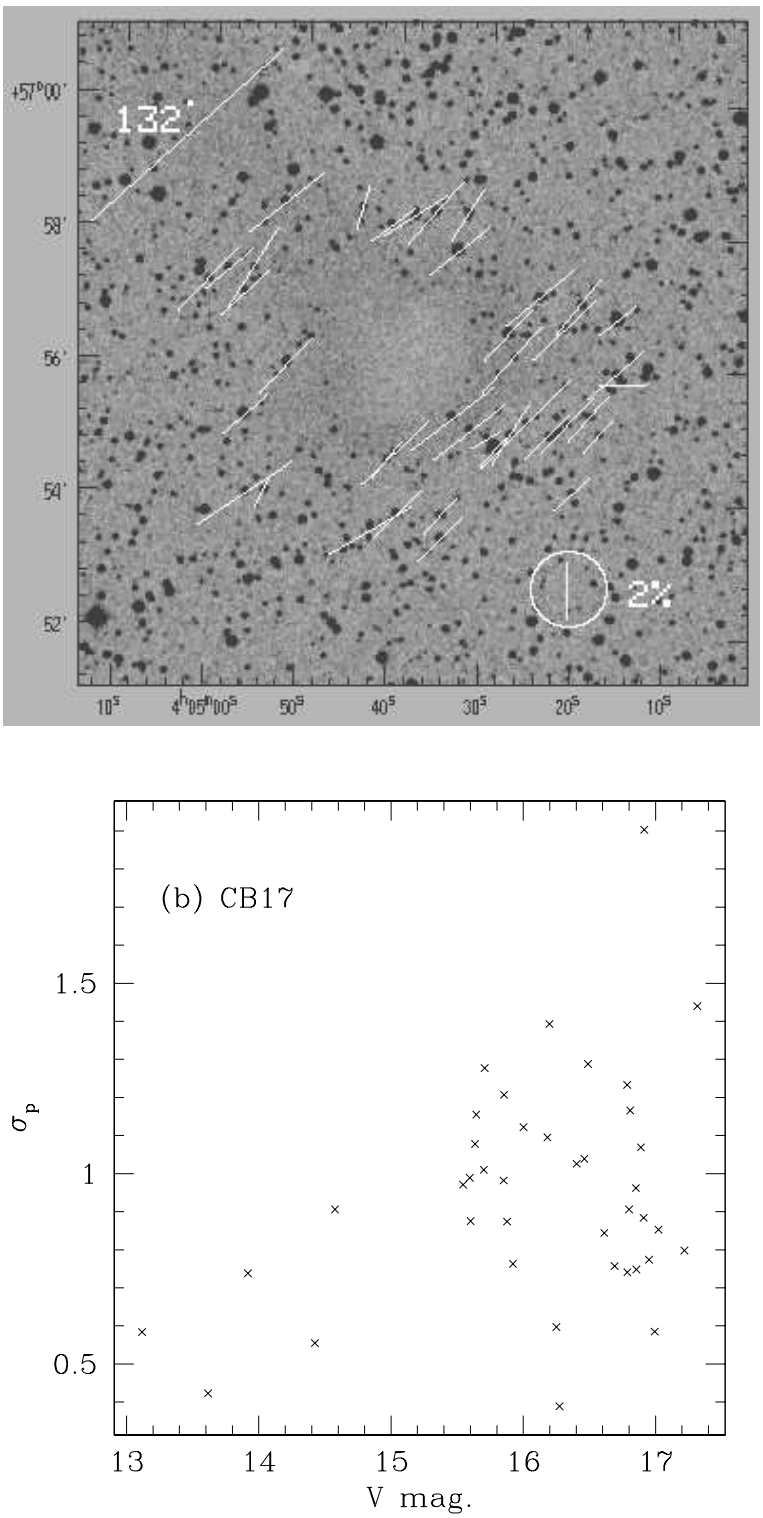

Figure 6.2: (Top) Polarization vector map of the field stars shining through the dust near the dark globule CB 17. (Bottom) Error in polarization measurement of each star plotted against its V-band magnitude.

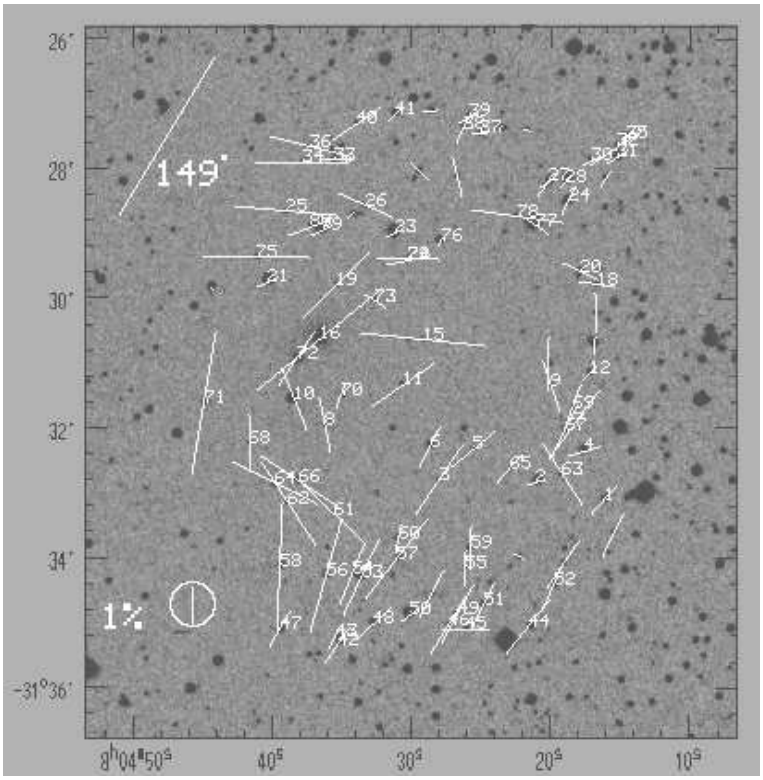

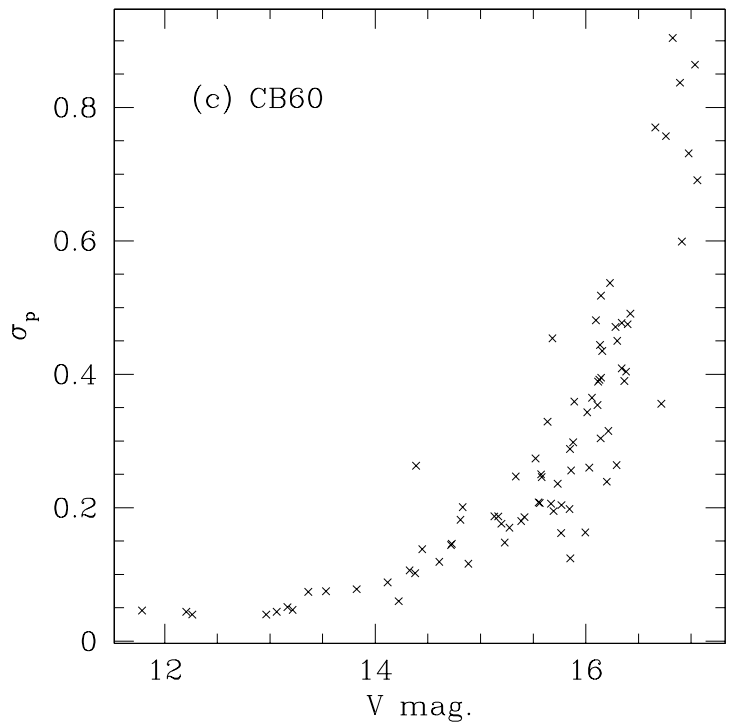

Figure 6.3: (Top) Polarization vector map of the field stars shining through the dust near the dark globule CB 60. (Bottom) Error in polarization measurement of each star plotted against its V-band magnitude.

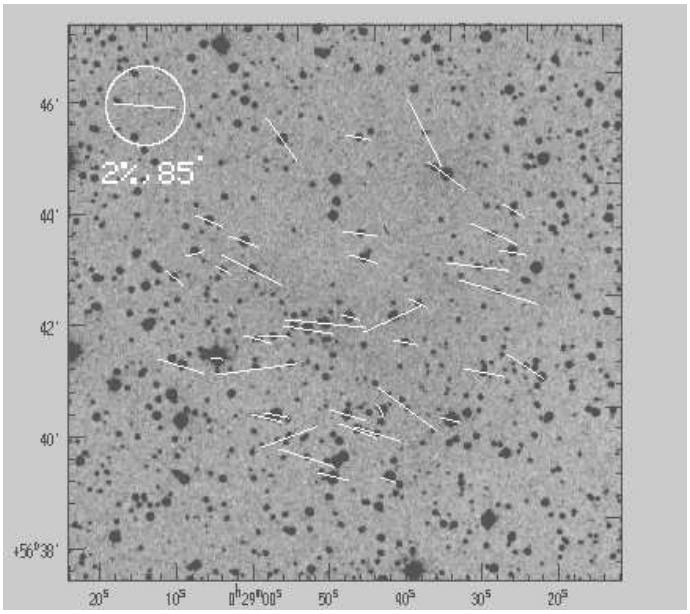

(a)

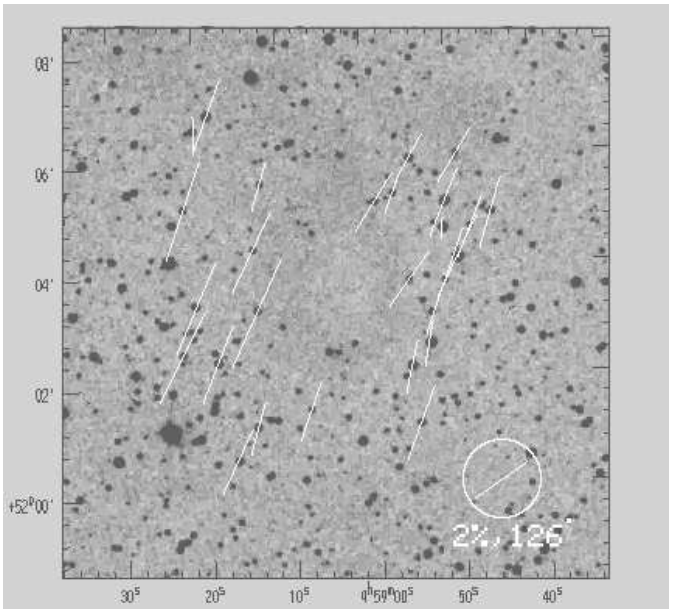

(b)

Figure 6.4: Polarization vector maps of the field stars shining through the dust near Bok globules (a) CB 3 and (b) CB 25. The circled vectors indicate the scale and correspond to 2% polarization. These vectors are marked approximately in the direction of the plane of the galaxy towards the regions.

Table 6.1: Linear polarization data of stars behind the clouds CB 16 and CB 17

(a) CB 16

No.	p (%)	σ_p (%)	θ (°)	σ_θ (°)	V mag
1	4.66	0.29	140.1	1.8	14.26
2	4.39	0.21	136.8	1.4	14.38
3	4.42	0.17	141.7	1.1	15.32
4	4.12	0.17	145.4	1.2	14.95
5	3.70	0.11	143.1	0.8	14.15
6	2.58	0.09	144.3	1.0	13.16
7	2.31	0.36	135.2	4.4	15.19
8	3.58	0.55	147.8	4.4	16.41
9	3.64	0.16	141.7	1.3	14.97
10	3.06	0.23	152.2	2.2	15.17
11	2.64	0.11	138.8	1.2	13.86
12	5.75	0.62	149.9	3.1	16.67
13	2.07	0.82	143.5	11.3	16.69
14	1.90	0.20	140.1	3.1	15.31
15	2.48	0.45	147.8	5.2	16.33
16	1.14	0.26	138.7	6.4	15.86
17	3.88	0.16	143.2	1.2	15.09
18	4.86	0.63	145.8	3.7	16.92
19	3.64	0.23	141.9	1.8	14.98
20	5.81	0.88	147.3	4.3	16.83
21	3.63	0.05	140.2	0.4	12.83
22	5.47	0.11	146.4	0.6	14.73
23	6.15	0.38	148.9	1.8	16.13
24	4.36	0.38	146.0	2.5	16.21
25	3.99	0.25	141.8	1.8	15.64
26	4.51	0.32	141.9	2.0	15.19
27	4.37	0.08	150.2	0.5	13.83
28	3.55	0.88	152.0	7.1	16.76
29	6.57	0.41	141.6	1.8	15.84
30	2.97	0.27	137.9	2.6	15.36
31	4.70	0.18	136.4	1.1	13.68

(b) CB 17

No.	p (%)	σ_p (%)	θ (°)	σ_θ (°)	V mag
1	2.18	1.12	135.1	14.7	16.00
2	3.34	1.23	118.9	10.6	16.79
3	2.28	0.87	134.7	11.0	15.88
4	3.89	1.29	123.7	9.5	16.49
5	1.68	0.58	134.0	10.0	16.99
6	1.29	0.58	137.1	12.9	13.12
7	2.40	1.21	148.6	14.4	15.86
8	3.10	1.39	128.6	12.9	16.20
9	2.66	0.96	135.7	10.3	16.85
10	4.41	1.44	135.3	9.4	17.32
11	2.16	1.10	137.8	14.5	16.18
12	3.60	0.98	127.1	7.8	15.85
13	2.00	0.56	131.8	7.9	14.42
14	1.67	0.39	94.2	6.7	16.27
15	2.50	0.99	131.0	11.3	15.60
16	2.61	1.01	137.8	11.1	15.70
17	3.19	0.77	138.4	7.0	16.95
18	2.47	0.91	136.7	10.5	14.58
19	3.00	0.88	133.1	8.4	15.60
20	1.66	0.42	129.5	7.3	13.62
21	2.46	0.76	139.9	8.9	15.92
22	2.97	1.15	129.7	11.1	15.65
23	2.28	0.74	134.4	9.3	16.79
24	3.01	0.91	138.1	8.6	16.80
25	3.36	0.75	147.0	6.4	16.85
26	2.17	0.80	132.1	10.5	17.22
27	2.68	0.74	129.0	7.9	13.92
28	1.91	1.03	125.8	15.4	16.40
29	2.58	0.60	122.6	6.6	16.25
30	2.15	0.76	147.3	10.1	16.69
31	2.95	0.97	137.8	9.4	15.55
32	3.28	1.04	129.4	9.1	16.46

Table 6.2: Linear polarization data of stars behind the cloud CB 60

No.	p (%)	σ_p (%)	θ (°)	σ_θ (°)	V mag	No.	p (%)	σ_p (%)	θ (°)	σ_θ (°)	V mag
1	1.01	0.12	137.2	3.3	14.89	41	0.52	0.10	129.6	5.6	14.38
2	0.43	0.08	108.4	5.3	13.82	42,1	1.17	0.28	145.4	6.9	15.31
3	2.24	0.54	145.0	6.9	16.23	43,1	0.75	0.20	153.7	7.8	15.10
4	0.88	0.14	103.3	4.7	14.72	44,1	1.83	0.14	141.0	2.2	14.44
5	1.51	0.44	128.4	8.3	16.15	45	1.25	0.57	90.0	13.0	16.33
6	1.17	0.14	152.2	3.4	14.45	46,1	1.80	0.41	147.8	6.4	16.48
7	2.29	0.90	143.4	11.3	16.83	47,1	1.12	0.13	148.0	3.3	14.15
8,2	1.49	0.44	11.6	8.5	16.13	48,1	1.27	0.61	129.5	13.7	15.43
9,3	1.38	0.49	17.3	10.2	16.42	49,1	1.77	0.47	152.7	7.6	15.94
10,2	1.79	0.05	20.2	0.7	13.22	50,1	0.57	0.08	123.6	3.9	13.10
11	2.05	0.26	124.9	3.7	16.29	51,1	1.28	0.28	154.2	6.2	15.09
12	0.43	0.19	134.2	12.9	15.69	52,1	1.40	0.13	156.5	2.7	15.33
13,3	1.46	0.18	178.9	3.5	15.39	53,1	2.24	0.14	155.6	1.8	15.01
14,3	0.49	0.12	179.8	6.9	14.61	54,1	1.73	0.19	157.9	3.1	14.87
15	3.41	0.48	83.9	4.0	16.34	55,1	0.97	0.36	179.0	10.6	16.16
16	4.36	0.05	129.4	0.3	13.17	56,1	3.16	0.21	165.0	1.9	14.76
17,3	1.09	0.47	2.0	12.4	16.28	57,1	2.66	0.41	142.6	4.4	15.58
18,4	0.96	0.20	82.6	6.1	15.77	58,1	3.44	0.14	177.7	1.2	14.81
19	2.47	0.52	134.2	6.0	16.14	59,1	1.15	0.54	175.9	13.3	15.82
20,4	1.08	0.15	66.8	3.9	15.23	60,1	0.72	0.30	169.8	11.8	15.64
21,4	0.62	0.04	115.9	1.8	12.97	61	2.27	0.94	48.1	11.8	16.63
22,4	1.67	0.40	86.9	6.8	16.15	62	2.65	0.61	32.6	6.6	16.24
23,4	0.53	0.04	118.9	2.4	12.21	63	2.01	0.47	33.1	6.7	15.92
24	0.88	0.06	154.1	1.9	14.22	64	2.55	0.12	64.2	1.3	14.83
25,4	2.79	0.19	84.9	1.9	15.42	65	0.97	0.50	139.1	14.8	16.41
26,4	1.58	0.34	66.7	6.2	16.01	66	2.50	0.15	56.4	1.7	14.72
27	0.62	0.11	129.3	4.9	14.33	67	1.49	0.44	152.5	8.6	15.67
28	0.38	0.07	128.9	5.6	13.36	68,2	1.57	0.48	2.1	8.8	16.23
29	1.05	0.41	13.0	11.2	16.34	69,3	1.31	0.23	161.9	5.1	15.50
30	0.55	0.26	115.5	13.5	16.03	70,2	0.74	0.16	157.9	6.2	15.30
31	0.67	0.09	126.1	3.8	14.12	71,3	3.86	0.18	170.5	1.4	14.92
32	1.79	0.47	124.1	7.6	16.40	72	1.72	0.10	145.6	1.6	14.20
33,4	0.69	0.18	86.5	7.3	15.20	73	0.68	0.35	60.5	14.8	15.43
34,4	2.55	0.39	90.7	4.4	16.37	74,4	1.14	0.59	102.2	14.8	16.02
35	0.84	0.16	138.6	5.5	15.99	75,4	2.82	0.20	89.9	2.0	14.95
36,4	2.19	0.84	76.0	10.9	16.89	76	0.32	0.13	152.4	11.8	14.73
37,4	0.44	0.20	94.7	12.9	15.85	77	0.80	0.17	58.8	6.0	11.11
38	0.81	0.16	155.2	5.8	15.77	78,4	2.49	0.37	82.4	4.3	16.63
39	0.65	0.17	127.2	7.5	15.27	79,4	0.58	0.02	119.3	0.9	12.12
40	1.51	0.73	125.7	13.8	16.98	80,4	1.30	0.18	112.6	3.9	15.58

Table 6.3: Linear polarization data of stars behind the clouds CB 3 and CB 25

(a) CB 3

No.	p (%)	σ_p (%)	θ (°)	σ_θ (°)	V mag
1	0.51	0.04	67.5	2.1	12.74
2	0.98	0.03	74.2	0.9	11.76
3	1.80	0.45	73.1	7.2	15.93
4	1.53	0.33	73.9	6.2	15.80
5	1.25	0.06	70.8	1.3	13.71
6	0.61	0.04	79.6	1.7	11.13
7	1.19	0.06	70.8	1.5	13.06
8	0.95	0.23	74.7	7.1	15.36
9	0.75	0.04	76.3	1.7	12.13
10	2.30	0.55	54.0	6.8	16.26
11	0.39	0.06	25.4	4.7	13.86
12	1.23	0.25	78.9	5.9	14.99
13	1.36	0.34	55.5	7.1	15.98
14	2.54	0.50	98.4	5.6	15.93
15	1.56	0.09	73.8	1.6	13.67
16	0.39	0.09	77.5	6.9	10.03
17	0.79	0.17	80.1	6.1	14.59
18	0.88	0.45	74.1	14.7	15.48
19	1.00	0.15	87.3	4.2	14.72
20	1.62	0.03	80.8	0.6	12.84
21	2.59	0.08	83.7	0.9	13.33
22	2.06	0.08	113.5	1.1	13.45
23	0.54	0.03	77.3	1.5	12.86
24	2.58	0.63	73.6	7.1	16.28
25	2.02	0.24	81.5	3.4	15.90
26	0.71	0.10	52.8	4.2	14.30
27	2.11	0.08	64.2	1.1	14.15
28	0.55	0.23	57.1	12.2	16.14
29	0.86	0.06	80.3	2.2	13.37
30	0.93	0.04	72.9	1.3	13.30
31	1.61	0.68	64.9	12.1	16.75
32	0.99	0.03	67.1	0.9	12.87
33	1.04	0.14	80.4	3.8	14.65
34	0.97	0.06	65.8	1.7	13.71
35	0.79	0.12	59.5	4.3	14.98
36	1.42	0.04	54.8	0.9	12.49
37	0.73	0.20	77.3	8.0	15.04
38	2.27	0.38	27.7	4.7	16.27
39	1.62	0.07	36.3	1.2	13.13

(b) CB 25

No.	p (%)	σ_p (%)	θ (°)	σ_θ (°)	V mag
1	2.21	0.33	155.9	4.2	15.18
2	2.48	0.40	160.5	4.6	15.67
3	1.71	0.24	163.3	4.0	15.46
4	1.94	0.93	161.6	13.7	16.69
5	1.71	0.23	168.1	3.9	14.04
6	2.61	0.12	159.0	1.4	14.74
7	3.35	0.57	153.4	4.9	15.92
8	1.44	0.05	170.8	0.9	12.96
9	3.76	0.43	156.2	3.3	15.96
10	3.23	0.13	156.7	1.2	14.75
11	3.55	0.72	160.3	5.8	16.56
12	2.15	0.88	143.8	11.7	16.76
13	2.97	0.06	154.1	0.5	12.65
14	2.78	0.50	154.4	5.1	15.97
15	0.62	0.10	172.8	4.5	13.97
16	2.10	0.43	159.9	5.9	16.09
17	2.33	0.44	163.4	5.4	15.72
18	3.34	0.27	162.1	2.3	15.78
19	2.27	0.07	158.5	0.9	13.94
20	2.22	0.22	147.6	2.9	15.73
21	1.27	0.57	161.1	12.8	16.32
22	1.65	0.70	164.3	12.1	16.37
23	1.80	0.17	150.9	2.7	14.82
24	2.04	0.76	150.2	10.7	16.63
25	1.07	0.31	2.3	8.3	15.40
26	2.46	0.10	159.8	1.2	13.94

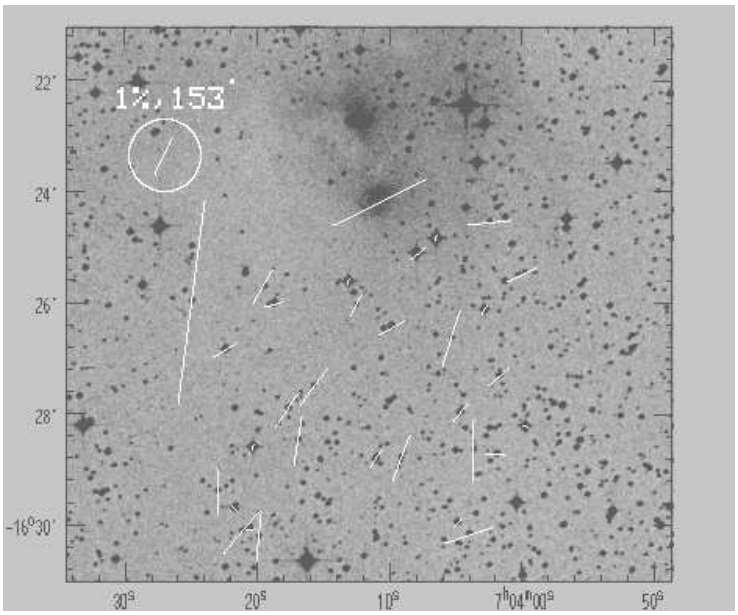

Figure 6.5: Polarization vector map of the field stars shining through the dust near Bok globules CB 54. The circled vector indicates the scale and correspond to 1% polarization. Its orientation indicates the the approximate direction of the Galactic plane towards this cloud.

Table 6.4: Linear polarization data of stars behind the cloud CB 54

No.	p (%)	σ_p (%)	θ (°)	σ_θ (°)	V mag
1	1.23	0.44	174.2	10.1	15.79
2	1.45	0.49	139.0	9.6	15.46
3	1.32	0.35	107.6	7.6	15.54
4	0.19	0.08	107.3	11.6	14.40
5	1.12	0.15	1.6	3.9	14.63
6	0.51	0.12	147.1	6.9	14.08
7	1.24	0.59	158.6	13.6	15.79
8	0.54	0.11	84.3	6.0	14.18
9	0.17	0.04	158.6	5.8	12.53
10	1.28	0.30	171.5	6.8	15.14
11	0.14	0.06	80.7	12.4	13.04
12	0.58	0.05	140.7	2.6	13.59
13	1.05	0.15	146.7	4.2	15.03
14	0.66	0.07	128.2	3.2	14.36
15	0.68	0.12	122.5	4.9	13.54
16	1.49	0.35	161.4	6.7	15.78
17	0.75	0.13	121.0	5.1	13.93
18	0.19	0.05	152.8	7.3	13.10
19	0.42	0.06	106.8	4.3	13.68
20	5.22	0.34	172.5	1.9	14.93
21	0.96	0.31	150.1	9.4	15.43
22	0.15	0.05	166.4	9.8	12.58
23	0.47	0.05	124.4	3.3	12.13
24	0.12	0.04	168.6	8.8	11.41
25	2.63	0.04	116.6	0.5	13.56

and CB 25 can safely be assumed to be occurring mainly at these clouds themselves. However, the same assumption may not be true in the case of CB 3, CB 54 and CB 60 because of the lower value of linear polarization and the large dispersion in position angles seen towards this cloud. Since the typical magnetic field decorrelation lengths in the Galaxy is about 300-400 pc, such large dispersion in position angles can also be due to light from distant stars behind these clouds, having to pass through several decorrelation lengths in the interstellar medium.

6.4 Discussion

6.4.1 Geometry of the magnetic fields

The most striking feature of the maps in Fig. 6.1-6.5, is the clear alignment of a majority of polarization vectors, in the case of CB 16, CB 17 and CB 25 and the lack of such a predominant alignment in the case of CB 3, CB 54 and CB 60. This feature is reflected in the histograms of polarization position angles, shown in Fig. 6.6 and 6.7, for the clouds.

The histograms for CB 16, CB 17 and CB 25 show narrow peaks close to the mean polarization direction. Such distinct maxima in polarization position angle histograms, seem to be the rule rather than the exception, for Galactic molecular clouds (MG). Nevertheless, what makes these clouds interesting are their particularly narrow number distribution of position angles. The rms deviation from mean of the polarization position angles is only about 5° in the case of CB 16, about 10° in CB 17 and about 8° in CB 25. However, if one of the stars (star no. 14 of Table 6.1(b)) towards CB 17, which shows an anomalous position angle of 94°, is culled from the calculation, the rms deviation for this cloud is reduced to about 7°. These dispersions are considerably smaller than the typical range of 12°-52°, usually observed in Galactic molecular clouds (MG). It should also be noted that a considerable contribution to this dispersion comes from errors in the measurement of individual polarization position angles.

The histogram of polarization position angles for CB 3 and CB 60 also show distinctly peaked structures. However, unlike in the other two clouds, this peak is offset by large angles from the mean position angles. Besides, the rms dispersion of the position angles about the mean is very large (46° and 27°) in these clouds, which indicates the lack of a preferred position angle of polarization vectors. On the other hand, a visual inspection of the polarization map of CB 60 (Fig. 6.3), does give an impression of some underlying pattern in the polarization vectors. Here, we describe, two tests which were made on the data, in an attempt to quantify these pattern, if it exists. Such quantification has become possible due to the availability of a large size sample of stars for which polarimetric measurements have been made.

Firstly, the centre of the field, over which the stars having polarimetry data is distributed, was determined. The equatorial coordinates of this point are 8:4:30.0 and -31:31:18 and is marked with a cross in the map of Fig. 6.3. With this point as centre,

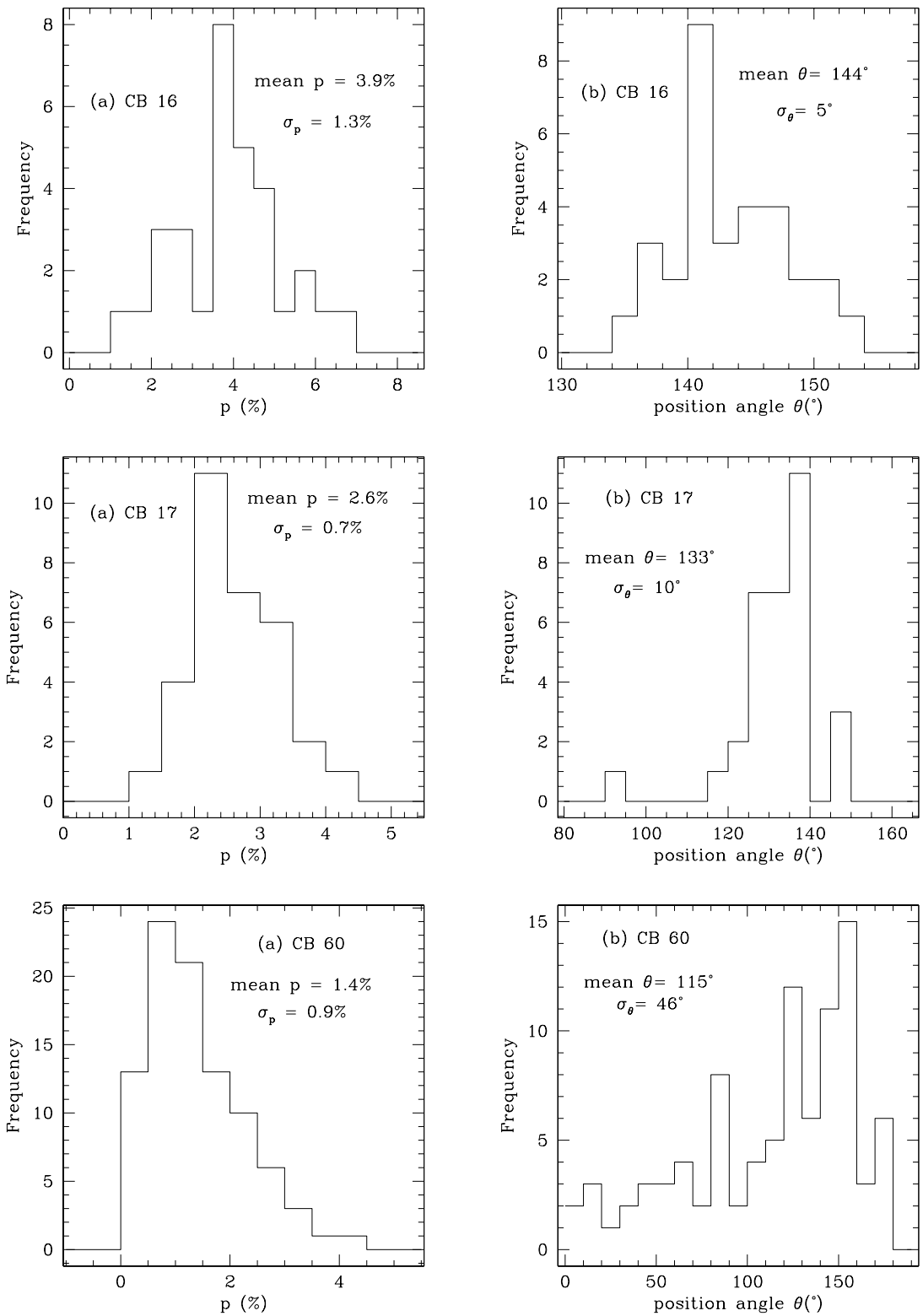

Figure 6.6: (a) Histogram of degree of linear polarization (p) for CB 16, CB 17 and CB 60. (b) Histogram of polarization position angles (θ) for the three clouds. σ_p and σ_θ are the rms dispersion from mean values of p and θ.

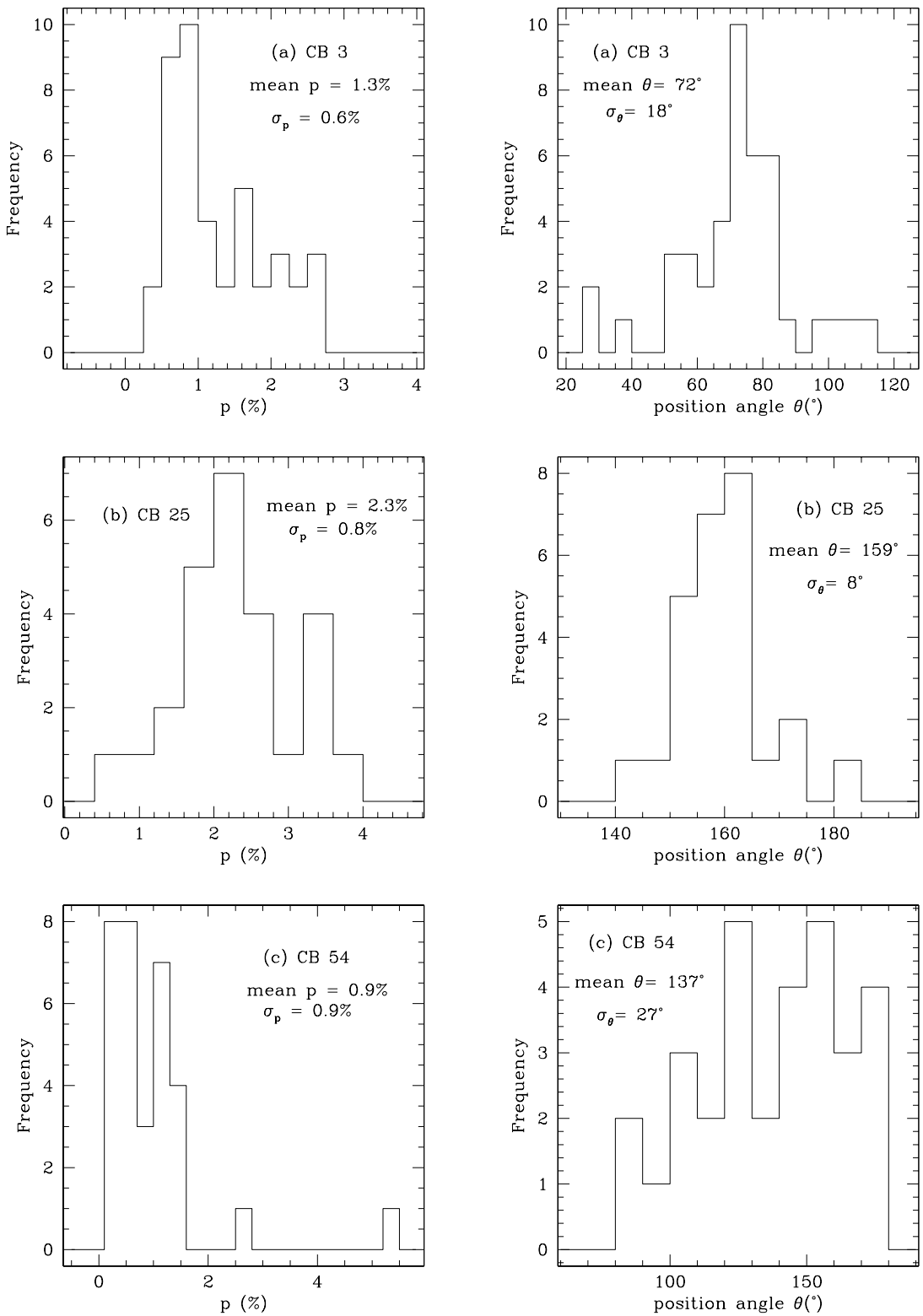

Figure 6.7: Histograms of degree of linear polarization (p) and polarization position angles (θ) for the clouds CB 3 (a), CB 25 (b) and CB 54 (c). σ_p and σ_θ are the rms dispersion from mean values of p and θ.

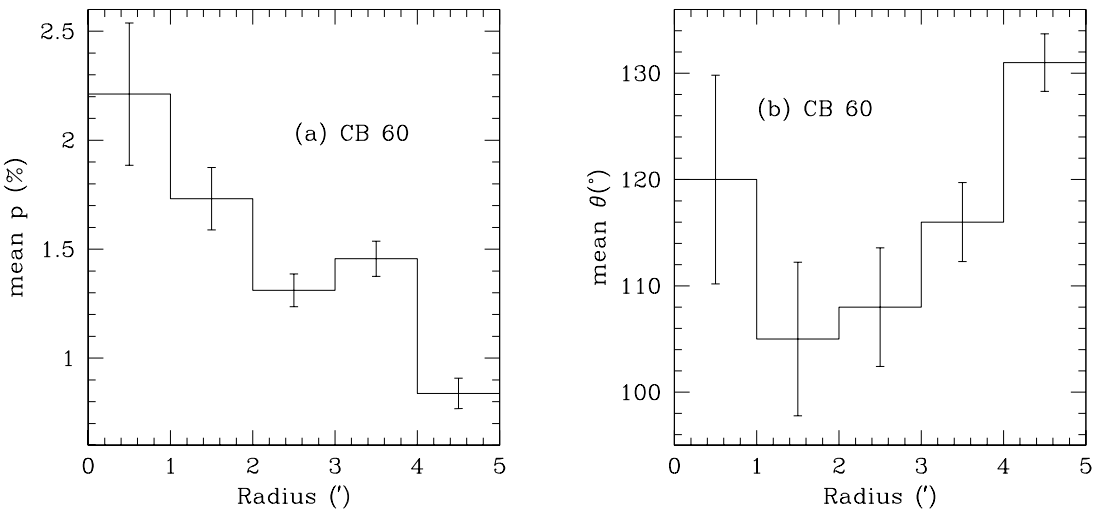

Figure 6.8: (a) Mean degree of linear polarization within radial bins away from the centre. (b) Mean polarization position angle within radial bins away from the centre.

concentric circular bins are superimposed on the polarization vector map. The means and the rms deviations from the means, of the degree of polarization and position angle of all stars in each radial bin are determined. Fig 6.8(a) shows a plot of mean polarization within each of the radial bins. There is a clear trend of decrease in average linear polarization ($< p >$) as one moves away from the centre, where $< p > \sim 2.2\%$, towards the periphery of the cloud about $4.5'$ away from the centre, where $< p >$ falls to about 0.8%.

The plot of mean position angles within radial bins away from the centre, also shows a definite pattern. Within each of the first four radial bins, (upto $4'$ away from the centre), the mean position angles and their rms dispersions from the respective means, are consistent with the global (calculated for all the stars in the cloud) mean position angle of 115° and the global rms dispersion of 46°. This feature probably indicates an underlying circular symmetry in the polarization vector pattern associated with the cloud. However, in the bin farthest from the centre, the mean position angle is about 131° and the rms dispersion from this mean is only 21°. This relatively higher value of the mean position angle (compare with the direction of the Galactic plane at 149°) and the lower value of dispersion, might be indicative of the growing influence of the ambient Galactic magnetic field in these regions. There also appears to be an increasing trend in the mean position angle, outwards from the second bin, noticeable in spite of the large dispersions.

In order to look for circular symmetry in the vector pattern, we divide the field into roughly four quadrants, defined by the NE-SW and NW-SE axes through the centre of the field. The stars chosen in each of these quadrants are marked with the corresponding quadrant number, on the map in Fig 6.3. The mean position angles and rms dispersions of stars in each of the four quadrants is given in Table 6.5. Remarkably, we see that each of these quadrants does show a definite preference of position angles,

Table 6.5: Mean and rms dispersion of position angles in four quadrants

Quadrant	1	2	3	4
$< \theta >$	154	0	92	1
σ_θ	14	12	16	17

Table 6.6: Mean properties of polarizations and position angles in the clouds

Cloud Name	$< p >$ (%)	σ_p (%)	$< \theta >$ (°)	σ_θ (°)	cloud major axis[a] (°)	size[a] (′)	Gal. plane (°)
CB 3	1.3	0.6	72	18	45	6.7×5.6	85
CB 16	3.9	1.3	144	5	100	6.7×2.2	132
CB 17	2.6	0.7	133	10	60	2.2×2.2	132
CB 25	2.3	0.8	159	8	0	2.2×2.2	126
CB 54	0.9	0.9	137	27	40	5.6×3.4	153
CB 60	1.4	0.9	115	46	40	10.1×6.7	149

[a]Ref: CB

as indicated by the low values of rms dispersions. This provides clear evidence for the presence of an underlying circular symmetry in the vector patterns.

6.4.2 Effect of/on magnetic fields on/of globules

Columns 2-5 of Tab. 6.6 list the global means and rms dispersions from the respective means of the degree of linear polarization and the position angles of stars in each of the clouds. Also listed are the position angle of the major axis of each cloud (as listed by CB) and the approximate direction of the Galactic plane towards it. The mean position angles of polarization vectors, for CB 16 and CB 17, appear to be coupled to the ambient magnetic field direction, indicated by the orientation of the Galactic plane. However, the major axes of the clouds do not show any relation to either of these directions. At least in the case of CB 16 and CB 17, it is evident that the processes leading to the formation of the globules have not affected the ambient magnetic field to any large extent. It is interesting to note here that while trying to understand the physical state of a very similar globule CB 4, Dickman and Clemens (1983) were able to provide satisfactory models for the equilibrium state as well as the slight ellipticity of the cloud, without introducing the effects of a magnetic field. In CB 25, the mean value of the polarization vector orientations is 159°. This does not appear to be strongly coupled to either the Galactic magnetic field in the region (assumed to be along the

Table 6.7: Results of *IRAS* photometry and ^{12}CO spectroscopy of the clouds[a]

	IRAS					^{12}CO J = 2 – 1		
CB No.	S_{12} (Jy)	S_{25} (Jy)	S_{60} (Jy)	S_{100} (Jy)	Area (arcmin.^{2})	T_R (K)	ΔV (kms^{-1})	group
3	9.2	9.4	67.62	222.81	199	6.43	3.08	C
16	1.27	1.12	2.43	18.44	70	5.93	0.84	A
17	0.79	0.93	3.66	16.72	62	5.24	0.99	A
25	0.36	0.15	0.82	8.31	23	4.29	0.7	A
54	4.47	8.06	69.69	179.71	125	6.26	4.51	C
60	9.55	12.02	54.39	177.76	121	12.88	1.82	B

[a]Ref: Clemens et al 1991

plane of the Galaxy which has a position angle of 126°) or the position angle of the major axis of the globule which is at 0° (CB).

The clouds in the sample identified by CB, have been studied with co-added IRAS photometry and ^{12}CO $J = 2 - 1$ spectroscopy by Clemens et. al. (1991). Table 6.7 contains an extract from the results of their study, which corresponds to the three clouds of interest here. Columns 2-5 are the net fluxes in the four *IRAS* bands and column 6 lists the area of the aperture used for photometry. ^{12}CO temperature and line-widths are listed in columns 7 and 8. Each of these columns illustrates the similarity between clouds CB 16, CB 17 and CB 25 and also how different CB 3, CB 54 and CB 60 are, compared to them. The classification in column 9 has been suggested by Clemens et. al. (1991) based on a plot of the CO temperature (T_R) of each cloud in their sample, against the CO line-width (ΔV). They find that the clouds distributes themselves into roughly three groups. About 74% of the clouds in their sample are classified as quiescent, given their low temperatures and line-widths ($T_R < 8.5$ K and $\Delta V < 2.5$ kms^{-1}). CB 16 and CB 17 fall in this group, which they call group A. The second group (B) is the smallest and contains about 9% of the clouds, which are relatively warmer $T_R > 8.5$ K, but with $\Delta V < 2.5$ kms^{-1}. CB 60 falls in this group. The observed excess infrared flux and larger size of CB 60 as compared to the other two clouds (Table 6.7), are properties typical of group B clouds. The remaining clouds form group C, which are dynamically more active ($\Delta V > 2.5$ kms^{-1}), but are cool ($T_R < 8.5$ K). CB 3 and CB 54 belong to this group.

At least three mechanisms have been suggested as possible causes for the higher temperatures of clouds in group B – excessive cosmic ray activity, gravitational collapse or thinness and/or clumpiness of the clouds allowing the UV component of the interstellar radiation field to penetrate deeper into the clouds. MG find evidence for larger dispersion in polarization position angles in clouds with embedded dense gas. Observations designed to detect dense ($n > 10^4$cm^{-3}) gas, using NH_3 and HC_3N as

tracers, failed to find evidence of any significant reservoirs of dense gas in CB 16, CB 17 and CB 25 (Kane et. al. 1994). The upper limits of mean densities in these clouds, were modeled to be about 5×10^3 cm^{-3} and no indications of core contraction were found in them. Another study of a subsample of the CB globules, aimed at detecting embedded Class 0 objects (André et. al. 1993), employing 3.6 cm continuum observations, led Yun et. al. (1996) to conclude that CB 17 and CB 25 do not show any signs of star-formation activity.

On the other hand, there is substantial evidence for the presence of at least one young stellar object (YSO) in CB 60 (Yun and Clemens 1990, 1994b). The position of this YSO (Yun and Clemens 1994b), coincides within a few arcseconds with the bright (V = 13.2) and heavily polarized (4.4%) star about 1.5′ east and 1′ north of the centre of the map in Fig. 6.3 (star no. 16 of Table. 6.2). In Fig. 6.9, we have bisected CB 60 into two halves, north and south of declination -31:31. Fig. 6.9(a) and (b) show the position angles of the stars in the southern half of the cloud, against their right ascension and declination coordinates respectively. We see that almost all stars (except 2, 4, 8, 9, 10, 45, 61, 62, 63, 64, 66, 68) cluster around a mean position angle of 151° with an rms dispersion of about 15°. The mean position angle is very close to the direction of the Galactic plane towards the cloud ($\sim$ 149°) and the dispersion is again similar to that has been observed in other molecular clouds (MG). These vectors, therefore, most probably trace the ambient Galactic magnetic field. Stars 8, 10, 61, 62, 64, 66 and 68, which form a separate group in Fig. 6.9(a) and Fig. 6.9(b), all lie within a circle of about 2.5′ radius, centred on the YSO. These stars have polarization position angles ranging from 0° to 60° and probably indicate that the magnetic field in this region has been affected by the star-forming process. These observations are consistent with earlier studies showing disturbed magnetic field patterns associated with Bok globules, harboring signs of star formation activity (Joshi et. al. 1985; Hodapp 1987).

Not many stars in the northern half of the cloud (Fig. 6.9(c) and (d)) seem to be aligned along the direction of the Galactic plane. This is understandable considering the fact that the YSO is in this half. However, the distribution of stars is bimodal, with one group having a mean of about 80° (rms dispersion 12°) and the other about 125° (rms dispersion 7°). There is a clear dearth of stars with intermediate position angles close to about 100°.

The polarization vectors associated with CB 3 and CB 54 also display a noticeably disturbed pattern when compared to those of the group A clouds. In particular, the polarization vectors along the south-western part of the core of CB 54 appear to form a circular arc with the vectors aligned along the edge of the cloud. Both CB 3 and CB 54 are known to Barbour IRAS point sources (CB), which have been identified to be associated with YSOs (Yun and Clemens 1994b). Bipolar molecular outflows are also present (Yun and Clemens 1992; 1994a), which have their centres quite close to the IRAS point sources found in the globules. Radio observations (Yun et al. 1996) also corroborate the presence of molecular cores in CB 3 and CB 54.

These observations clearly indicate that the nature of the magnetic fields associated with the Bok globules are closely related to the temperature and dynamic state of

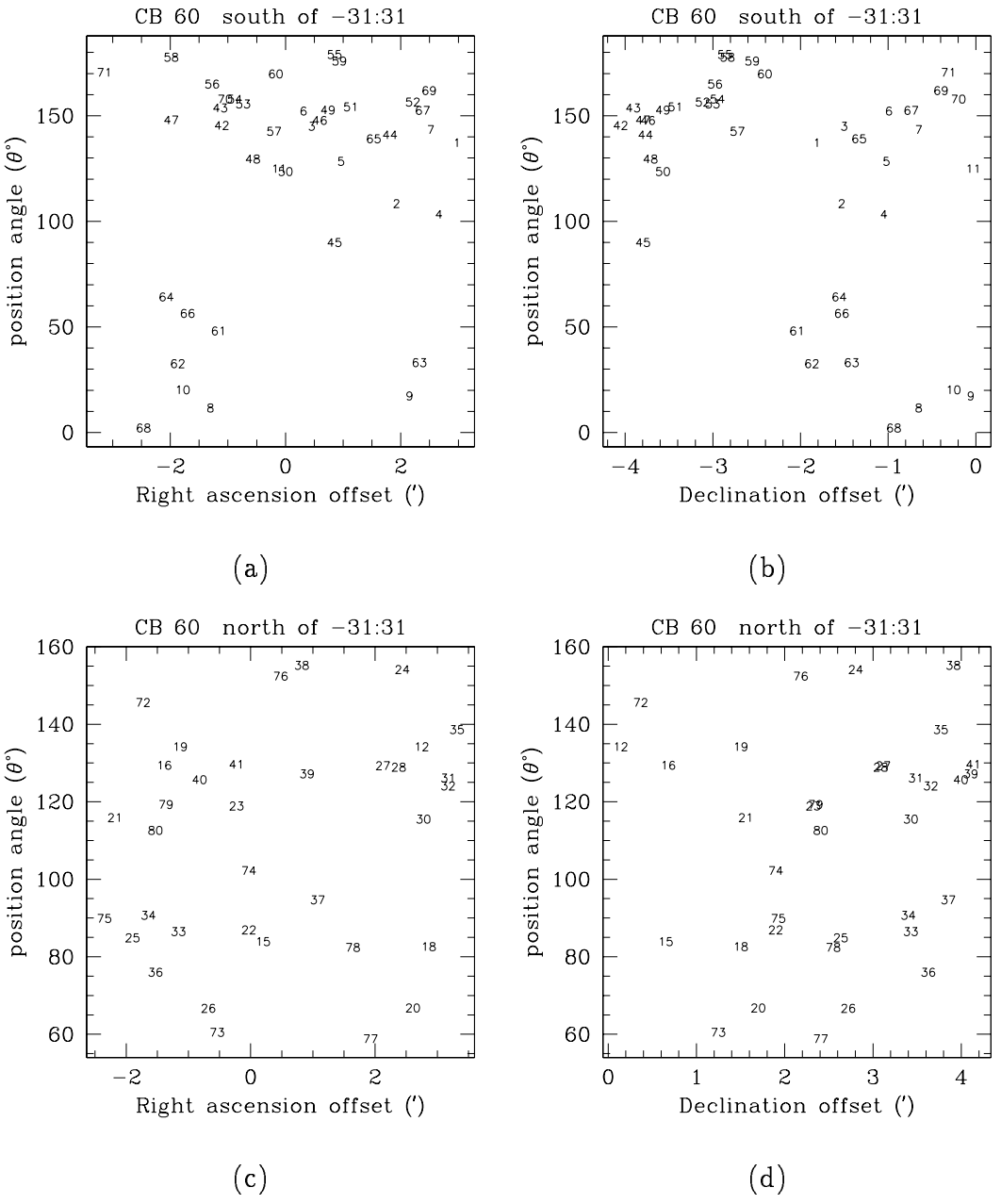

Figure 6.9: (a) polarization position angles plotted against the right ascension coordinates for stars in CB 60 south of declination -31:31. (b) polarization position angles plotted against the declination coordinates for stars in CB 60 south of declination -31:31. (c) polarization position angles plotted against the right ascension coordinates for stars in CB 60 north of declination -31:31. (d) polarization position angles plotted against the declination coordinates for stars in CB 60 north of declination -31:31.

these clouds. The high uniformity of the magnetic fields in the quiescent Bok globules and their alignment along the apparent directions of the local Galactic magnetic fields provide evidence that these fields have a role in the formation of the globules. It is also clear that the magnetic fields are involved in the processes of core-collapse and star-formation which occurs in many of the globules. However, polarimetry alone is not sufficient to fully understand these processes, but it has to be complemented by better estimates of distances to these clouds, extinction measurements as well as observations at millimeter and radio wavelengths, in order to obtain a complete picture of the processes involved.